The International Journal of Cardiovascular Imaging
https://doi.org/10.1007/s10554-020-01954-x

REVIEW PAPER

Physiology and coronary artery disease: emerging insights from computed tomography imaging based computational modeling

Parastou Eslami[1] · Vikas Thondapu[1] · Julia Karady[1] · Eline M. J. Hartman[2] · Zexi Jin[1] · Mazen Albaghdadi[3] · Michael Lu[1] · Jolanda J. Wentzel[2] · Udo Hoffmann[1]

Received: 2 June 2020 / Accepted: 23 July 2020

Abstract
Improvements in spatial and temporal resolution now permit robust high quality characterization of presence, morphology and composition of coronary atherosclerosis in computed tomography (CT). These characteristics include high risk features such as large plaque volume, low CT attenuation, napkin-ring sign, spotty calcification and positive remodeling. Because of the high image quality, principles of patient-specific computational fluid dynamics modeling of blood flow through the coronary arteries can now be applied to CT and allow the calculation of local lesion-specific hemodynamics such as endothelial shear stress, fractional flow reserve and axial plaque stress. This review examines recent advances in coronary CT image-based computational modeling and discusses the opportunity to identify lesions at risk for rupture much earlier than today through the combination of anatomic and hemodynamic information.

Keywords Computational fluid dynamics · Coronary computed tomography angiography · Plaque burden · Pathophysiology · Endothelial shear stress · Patient-specific modeling

Introduction

Despite the advances in medical therapy and development in cardiovascular invasive and noninvasive diagnostic testing, cardiovascular disease remains the number one cause of death worldwide [1]. Of these deaths, the majority of them are from coronary artery disease (CAD) and stroke [2]. In United States alone, by year 2035, the number of people with CAD is expected to grow to approximately 24.1 million, an additional ~ 8 million patients since year 2015, still remaining the leading cause of death [3]. This is largely due to the silent atherosclerotic plaque progression towards erosion or rupture, clinically presenting as acute coronary syndrome (ACS).

Major efforts in cardiovascular imaging have improved plaque assessment based on coronary anatomy to predict future atherosclerotic cardiovascular disease on a per patient basis. These include large clinical trials demonstrating noninvasive coronary computed tomography angiography (CTA) as a powerful prognosis imaging tool. Coronary CTA allows for noninvasive assessment of atherosclerotic coronary plaques by providing information regarding the coronary tree and the plaques morphology beyond simple narrowing. In the CONFIRM (COronary CT Angiography EvaluatioN For Clinical Outcomes: An InteRnational Multicenter Registry) trial, both plaque burden (C-index 0.64, $p < 0.0001$) and stenosis > 50%(C-index 0.56, $p = 0.002$) assessed on CTA particularly in proximal segments added incremental prognosis value to the traditional clinical risk score [4]. The PROMISE (Prospective Multicenter Imaging Study for Evaluation of Chest Pain) trial also demonstrated that coronary plaque anatomy assessment based on CTA when stratified to mild, moderately, or severely abnormal, when compared with normal assessments, the hazard ratios of having events increased proportionally (2.94, 7.67, 10.13, all $P < 0.001$) [5]. A secondary analysis in the PROMISE trial also showed that plaque morphology and high-risk plaques based on CTA although strong prognosis predictors of events, they are not

✉ Parastou Eslami
peslami1@mgh.harvard.edu

[1] Department of Radiology, Massachusetts General Hospital, Harvard Medical School, Boston, MA, USA

[2] Department of Cardiology, Biomedical Engineering, Erasmus MC, Rotterdam, The Netherlands

[3] Department of Cardiology, Massachusetts General Hospital, Harvard Medical School, Boston, MA, USA

Published online: 10 August 2020

as strong in predicting the vulnerable lesions [6]. Similar conclusions were made based on other larger clinical trials such as the SCOT-Heart (Scottish COmputed Tomography of the HEART Trial) [7] and ICONIC (Incident COroNary Syndromes Identified by Computed Tomography) [8] trails showing lower sensitivity of high-risk plaque features based on coronary anatomy in identifying the vulnerable lesions. Hence, the ability to identify lesions prone to erosion or rupture early on has been a specific goal of cardiovascular medicine for decades and atherosclerotic plaque characterization using CTA will continue to be an active area of research.

Atherosclerosis is a highly complex disease and the cascade of this disease development and progression involves cycles of disruption to physiologic flow, endothelial dysfunction, lipid accumulation, arterial inflammation, and vascular remodeling leading to development of plaque, its progression and finally rupture [9, 10]. As mentioned, coronary plaque anatomy delivers important information about the degree of stenosis and insights into morphology of the plaque. However, the lesion specific predictive value of this information to a clinical event due to erosion or rupture remains extremely low. Thus, combination of anatomy with physiology may be considerably more powerful in predicting lesion specific future acute coronary events [11, 12].

Among the physiologic measures that can be obtained are fractional flow reserve (FFR)—measured to identify coronary lesions for significantly limiting the blood flow to the myocardium [13–15]. Moving beyond flow limitation, the anatomic and physiological characteristics of a plaque may provide novel insights and understanding of pathophysiology of plaque with the potential to better treatment and management of patients with CAD [16]. For example, endothelial shear tress (ESS) based on invasive coronary imaging has been shown to be linked with atherogenesis, plaque progression and vulnerability in addition to platelet and leukocyte activation [17–21]. ESS is calculated via computational fluid dynamics (CFD) where hemodynamics is simulated in realistic models of coronary arteries. Additional hemodynamic derived factors such as axial plaque stress (APS) [22], plaque structural stress modeling tissue behavior (PSS) [21] and transluminal attenuation gradient [23, 24] have also been studied in relationship to CAD and coronary events.

Traditionally, using CFD, hemodynamic factors are assessed via invasive coronary imaging such as coronary angiograms coupled with intravascular ultrasound (IVUS) or optical coherence tomography (OCT). Coronary CTA, however, permits the noninvasive evaluation of the coronary atherosclerotic plaque and the 3D anatomy of the coronary trees. With advances in coronary CTA, it now has the temporal and spatial resolution to capture the lumen, plaque type and coronary wall allowing for patient-specific image based assessment of hemodynamics via computational modeling [25–27]. The ability to utilize CTA images to calculate the hemodynamics via CFD and identifying high-risk plaques beyond the coronary lumen and plaque will significantly empower this technique towards development of personalized medicine enabling therapeutic interventions stratified based on plaque characteristics. In this review we will explore the role of hemodynamics in evolution of CAD as reflected by plaque progression and vulnerability focusing on the contribution of coronary CTA and image-based computational modeling on the prospective identification of high-risk coronary lesions.

Image-based computational fluid and solid mechanics

Blood flow and tissue behavior can be modeled via constitutional mathematical equations that describe these behaviors. For example, with the proper input and output boundary conditions and patient anatomical 3D reconstructions based on imaging, coronary blood velocity and pressure can be computed solving the governing equations of fluid dynamics, known as the Navier–Stokes equations. Once the blood flow is solved in the coronaries, then hemodynamic parameters such as FFR, ESS, APS, etc. can be derived during post-processing steps. Similarly, finite element analysis (FEA) is based on solution of partial differential equations that describe the mechanics of coronary plaque and the resulting stresses in the coronary walls upon exposure to blood pressure. By prescribing realistic tissue geometry and elastic mechanical properties, it is possible to derive various internal tissue stresses. Fluid structure interaction (FSI) is a combination of fluid and solid mechanics allowing for simultaneous analysis of solid and fluid domains such as interaction of blood flow and coronary lesions. Recent advances in computational modeling provides a platform for such image-based computational analysis to become increasingly applicable to relevant clinical problems given advances in both computational power and coronary imaging. In the following sections, we will examine different hemodynamic parameters derived from CFD and FEA analysis based on coronary CTA imaging.

Hemodynamic Indices

FFR, originally defined as the maximal myocardial blood flow through a stenosed artery versus the hypothetical flow in the normal vessel—is perhaps one of the most well-known and widely practiced physiologic indices in the clinics. However, due to unknown "normal" blood flow information through the un-stenosed artery, it was

reformulated to be the ratio of pressure across a lesion in hyperemic condition. FFR first coined by Pijls et al. [13] in 1996 is traditionally obtained invasively through a pressure wire and to date is the gold standard diagnostic hemodynamic factor for ischemia detection [14, 28] which is performed in hyperemic conditions. In 1978 Gould [29] studied pressure drop in stenosed arteries in canine models introducing the concept of quantitative flow ratio (QFR) as a potential clinical application concluding flow response during coronary hyperemia is a quantitative measure for physiological assessment of coronary stenosis and flow reserve. QFR, (Medis medical imaging system, The Netherlands) has been recently proposed as an alternative way to measure FFR by the means of 3D quantitative coronary angiography (QCA) and thrombolysis in myocardial infarction frame counting [30]. In Wire-Free Functional Imaging II (WIFI II), a sub-study of Danish Study of Non-Invasive Diagnostic Testing in Coronary Artery Disease (Dan-NICAD study), in a total 240 lesions, QFR correctly classified 83% of the lesions using FFR with cutoff at 0.80 as a reference standard [31]. Instantaneous wave-free ratio (iFR) is another pressure-derived hemodynamic index defined as ratio of diastolic coronary and aortic diastolic "wave-free" period [32] which can be obtained at rest without the use of vasodilators. In the SWEDHEART [33] (Swedish Web-Based System for Enhancement and Development of Evidence-Based Care in Heart Disease Evaluated According to Recommended Therapies) and DEFINE-FLAIR [34] (Functional Lesion Assessment of Intermediate Stenosis to Guide Revascularization) trials, iFR showed non-inferiority to FFR in prognosis of significance of coronary artery stenosis [32]. The underlying assumption of the iFR technique is that resistance at rest conditions is equivalent to time-averaged resistance during FFR measurements, however, the diastolic resting myocardial resistance does not equal mean hyperemic resistance which raised some controversy in the literature [35]. It should be noted that FFR and iFR as pressure-derived indices are recommended by clinical practice guidelines such as American College of Cardiology and European Society of Cardiology for decisions on percutaneous coronary intervention procedures. Lastly, coronary flow reserve (CFR)-defined as the ratio of the hyperemic flow to the resting flow in a vessel—is a flowrate-based index which reflects flow limitations across the entire coronary circulation system including the microcirculation [36]. CFR is also an invasive measurement and in 737 vessels, low categorical CFR values were shown to be an independent predictor of vessel-oriented composite outcome (composite of cardiac death, vessel-specific myocardial infarction, and vessel-specific revascularization) in the high FFR groups (hazard ratio (HR) 4.99. 95% CI 2.104 to 11.879, $p < 0.001$) [36].

Fractional flow reserve-CT

Recently, patient-specific CFD modeling has been applied to coronary CTA enabling calculation of FFR, noninvasively without additional imaging—termed as FFR_{CT}. In the Diagnosis of Ischemia-Causing Stenosis Obtained Via Noninvasive Fractional Flow Reserve (DISCOVER-FLOW) study, one of early studies of FFR_{CT}, on a per-vessel basis, FFR_{CT} showed an accuracy, positive predictive value and a negative predictive value of 84.3%, 73.9% and 92.2%, respectively [27]. In patients with stable CAD scheduled to undergo invasive angiography, the investigators in the NXT (Analysis of Coronary Blood Flow Using CT Angiography: Next Steps) study showed a significantly better area under the receiver-operating characteristic curve for FFR_{CT} (AUC = 0.90) versus standard coronary CTA (AUC = 0.81) [37]. Moreover, they reported a per-vessel sensitivity and specificity of 84% and 86%, respectively. In a more recent study, in the PROMISE trial, among patients with stable chest pain, an $FFR_{CT} \leq 0.80$ was shown to be a significantly better predictor for recalculation of major averse cardiac events (MACE) than severe CTA stenosis ($p < 0.033$) [25]. FFR_{CT} is now approved by the United States Food and Drug Administration for functional evaluation of CAD and is currently commercially available. In addition, the United Kingdom's NICE (National Institute of Health and Care Excellence) has updated their chest pain guidelines which recommend coronary CTA as the initial diagnostic test for patient with stable chest pain and suspected CAD where FFR_{CT} has been mentioned as a safe with high accuracy technology [38, 39]. Therefore, CTA has shown a tremendous potential as an imaging modality to study hemodynamics via CFD.

Besides FFR_{CT}, other hemodynamic indices mentioned above (i.e. iFR and QFR) remain to be calculated based on invasive imaging and methodologies. Future CT-based calculations of these indices and their comparison with FFR_{CT} in diagnosing of patients with stable chest pain can shed the light into further computational calculations of hemodynamic indices based on CTA.

Biomechanical and Pathophysiological Forces

The vast majority of the evidences based on CTA are studies for CFD computed FFR. Although FFR and stress distributions are gained through CFD simulation, their derivation differs slightly. Blood velocity and pressure are calculated by CFD simulation (from which FFR is directly derived), but stress distributions are calculated based on the raw data

during post-processing steps. When blood flows through an artery it exerts three kinds of biomechanical stress of axial, circumferential, and shear contributing to the overall biomechanical strain distribution within vascular tissue. These stresses accumulatively are responsible for maintaining the arteries shape and regulating arterial wall function.

Endothelial shear stress-CT

ESS is the tangential force generated by the friction of blood flowing on the endothelial surface of the arterial wall and is proportional to fluid viscosity and the gradient of the velocity of the blood at the wall. In a cardiac cycle, due to flow pulsatility, complex vessel anatomy such as curvature, branching and obstructions, dynamic motion of the arteries as well as dynamic changes in coronary perfusion, local blood velocity changes in magnitude and direction. These alterations can result in locations with abnormally low or high ESS with flow disturbance, turbulence and flow reversal initiating endothelial cell dysfunction (Fig. 1). Consequently, as a result of this flow-induced endothelial injury and arterial inflammation, early atherosclerosis forms in

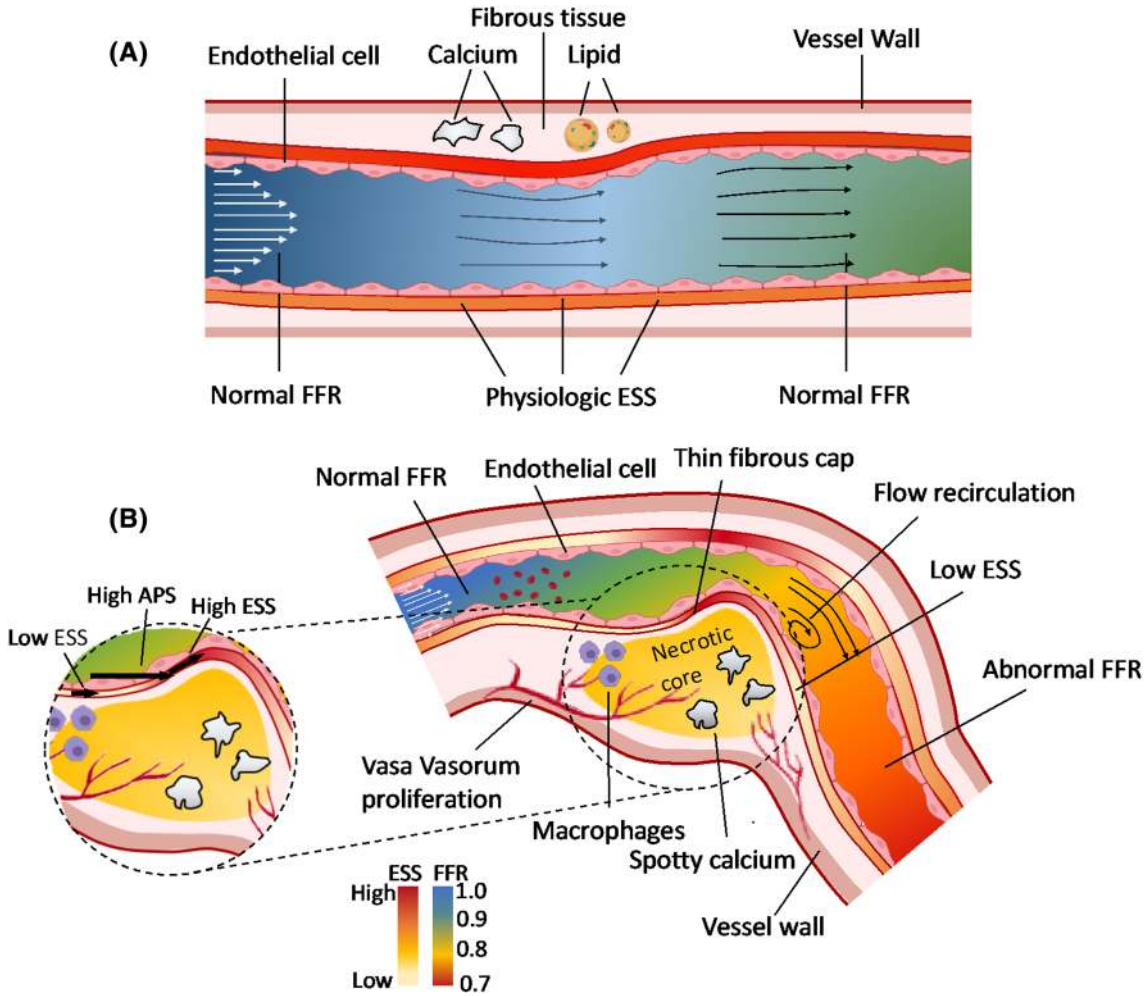

Fig. 1 A schematic illustration of interaction of physiological conditions and biomechanical stresses contributing in regulation of atherosclerosis. Morphology and functional characteristics of stable vulnerable plaque **a** with stable calcification and small lipid pools. The plaque leads to mild narrowing of the lumen with no disruption to the flow and no ischemia after the lesion (FFR > 0.8; green). ESS near the plaque is normal and in physiologic range. **b** Rupture prone vulnerable plaque with a large lipid-rich necrotic core, neovascularization, spotty calcium, thin fibrous cap and presence of inflammatory cells (macrophages). In the positively remodeled vessel wall at the site of plaque, the lesion causes severe luminal narrowing resulting in ischemia (FFR < 0.8; red). The lesion also causes flow disruption causing low ESS proximal to the lesion, low and oscillatory ESS distal to the lesion and high ESS at the neck of the lesion. The upstream low ESS at the shoulder of the plaque is more inflamed (indicated by presence of macrophages) whereas the downstream plaque region with low and oscillatory ESS promotes plaque growth. The heterogenous nature of ESS along the lesion may be the contributing factor in destabilization of the plaque and future ruptures. Since this is an upstream dominant plaque, the APS is high at the upstream shoulder adding to stresses promoting rupture. FFR: fractional flow reserve; ESS: endothelial shear stress; APS: axial plaque stress

these regions. Similar to APS and PSS, direct in-vivo measurements of ESS is not possible. Therefore, ESS is derived from 3-dimensional reconstruction of coronary arteries and CFD simulations of blood flow in these arteries.

Thus far, the majority of research studies performed has been based on invasive coronary angiograms coupled with IVUS and OCT [9, 19, 40, 41]. The purpose of this review is to provide insights in study advancements of ESS related pathology as derived from coronary CTA. However, to understand ESS and its association with plaque morphology, we will briefly discuss the important role that ESS plays in the pathophysiology of CAD.

ESS, plaque biology, progression and rupture

Animal studies

The pathophysiological role of ESS (high, low and oscillatory) was debated starting in late 1960s and early 1970s. In 1968, Fry [42] studied fluid dynamics in the thoracic aorta of dogs and reported that exposure to high shear stress resulted in deterioration of endothelial surface consisting of endothelial cytoplasmic swelling, cell deformation, degeneration and finally erosion of cell substance. Additionally, the influence of low and oscillatory ESS on atherosclerotic plaque initiation and progression was first described in 1971 by Caro et al. [43]. However, in-vivo computational modeling was not at the capacity to conduct a study that would calculate ESS measurements in association with pathophysiology of CAD. In arteries including the coronaries with undisturbed blood flow and physiological ESS, endothelial cells express atheroprotective genes and suppress proatherogenic genes leading to vascular quiescence. However, in a region with disturbed flow, such as outer edges of branching segments, highly curved segments or distal to stenosis, due to flow separation and secondary flows, low ESS disrupts endothelial function and triggers proatherogenic gene expression [44–46]. Once the plaque is formed and results in a stenosis, there is a positive feedback loop caused by flow disruption where a heterogeneous ESS pattern forms with low ESS at upstream shoulder of the plaque, low and oscillatory ESS downstream to the stenosis and high ESS at the neck of the stenosis. The persistent low ESS reduces nitric oxide production, increases low density lipoprotein (LDL) uptake, promotes endothelial cell apoptosis, and induces local oxidative stress and inflammation stimulating an atherogenic endothelial phenotype and subsequently leads to acceleration of atherogenesis and plaque vulnerability [9, 47] (Fig. 1b). In serial IVUS studies of coronary arteries studies of diabetic pigs, the majority of vulnerable plaques developed in vessel segments with low ESS [9, 41, 48]. In addition, the magnitude of low ESS at baseline was significantly associated with the severity of high-risk plaque features at follow up [49]. In a more recent animal study, in hypercholesterolaemic pigs, a more detailed analysis of ESS showed low and multidirectional ESS promote both initiation and progression of coronary atherosclerotic plaques [17].

Human studies

Invasive coronary angiography and IVUS

Human studies also showed a consistent pattern. The first pilot studies in 2000s based on intracoronary imaging and biplanar angiography showed regions of low ESS developed progressive atherosclerosis and outward remodeling in native and stented arteries [50, 51]. Other natural-history IVUS study in humans followed up where twenty patients with CAD underwent baseline and 6-month virtual histology IVUS (VH-IVUS) follow up. Low ESS segments developed increased plaque area and necrotic core as well as constrictive remodeling, whereas high ESS segments developed greater necrotic core and regression of fibrous and fibrofatty tissue resulting in a more constrictive remodeling in low compared with high ESS segments in follow-up [20]. In a larger study from the Prediction of Progression of Coronary Artery Disease and Clinical Outcome Using Vascular Profiling of Shear Stress and Wall Morphology (PREDICTION) trial, a total of 506 patients with ACS underwent three-vessel IVUS examination and had a 1-year follow up [18]. The results of this study demonstrated that independent of plaque morphology at baseline, in a subset of 374 patients low ESS can predict plaques that progressively enlarge and develop substantial lumen narrowing [18]. In the Providing Regional Observations to Study Predictors of Events in the Coronary Tree (PROSPECT) trial 697 patients with ACS underwent 3-vessel intracoronary imaging and were assessed after 3.4 years follow up. In the 97 patients that were analyzed in this trial, local ESS showed a strong association with MACE and no lesion without low ESS led to non-culprit MACE during follow-up, regardless of plaque burden, minimal lumen area, or lesion phenotype at baseline [19]. In the Fame II (Fractional Flow Reserve Versus Angiography for Multivessel Evaluation II) among 441 patients with FFR ≤ 0.80 who were randomized to medical therapy alone had 3 years of follow up for cardiac events. 29 patients with myocardial infarction (MI) were matched with a control group (n = 29) who did not have MI to study ESS in the coronary lesions. However, in this study in patients with stable CAD, high ESS proximal to the lesion had a significant incremental value to FFR in predicting myocardial infarction [52].These detailed observations highlight the importance of ESS-whether high or low in natural history and progression of CAD.

Noninvasive coronary CTA

Three dimensional (3D) coronary geometry visualization by coronary CTA enables CFD to calculate ESS-CT and subsequent coronary plaque behavior assessment (Fig. 2). In fact, more recently, ESS-CT has become an attractive avenue. In 72 patients with ACS, continuous ESS-CT as well as FFR_{CT} and axial plaque stress were studied to define an adverse hemodynamic characteristics and showed to have an incremental discriminant and reclassification ability for prediction of ACS [53]. In another CTA based study, in 100 patients who underwent CTA and invasive coronary angiography, high ESS was associated with adverse plaque characteristics (i.e. low attenuation plaque, positive remodeling, napkin-ring sign, and spotty calcification) independent of stenosis severity [54]. Despite promising evidence to assess ESS based on CTA, a more detailed study comparing CTA to the higher resolution invasive imaging modalities should be performed to provide more assurance that CTA captures the same ESS pattern as invasive imaging modalities (Fig. 3a–h. The fact that both low and high ESS have been associated with plaque vulnerability and ACS with ischemia demonstrates the complexity of fluid flow around the plaques and suggest that high or low ESS may be both responsible and it is the heterogeneous nature and gradient of ESS that destabilizes the plaque; hence rupture may occur at the site of both levels of ESS. In addition, mapping ESS distribution in each cross-section of plaque can inform us about the association of multidirectional ESS and plaque morphology characteristics such as large plaque volume, low CT attenuation, napkin-ring sign, spotty calcification and positive remodeling (Fig. 3i–k).

Prevention of MACE is challenging as over 50% of patients with MACE have no prior symptoms of myocardial ischemia or manifestations of CAD [55]. The development of MACE in patients without prior symptoms is commonly

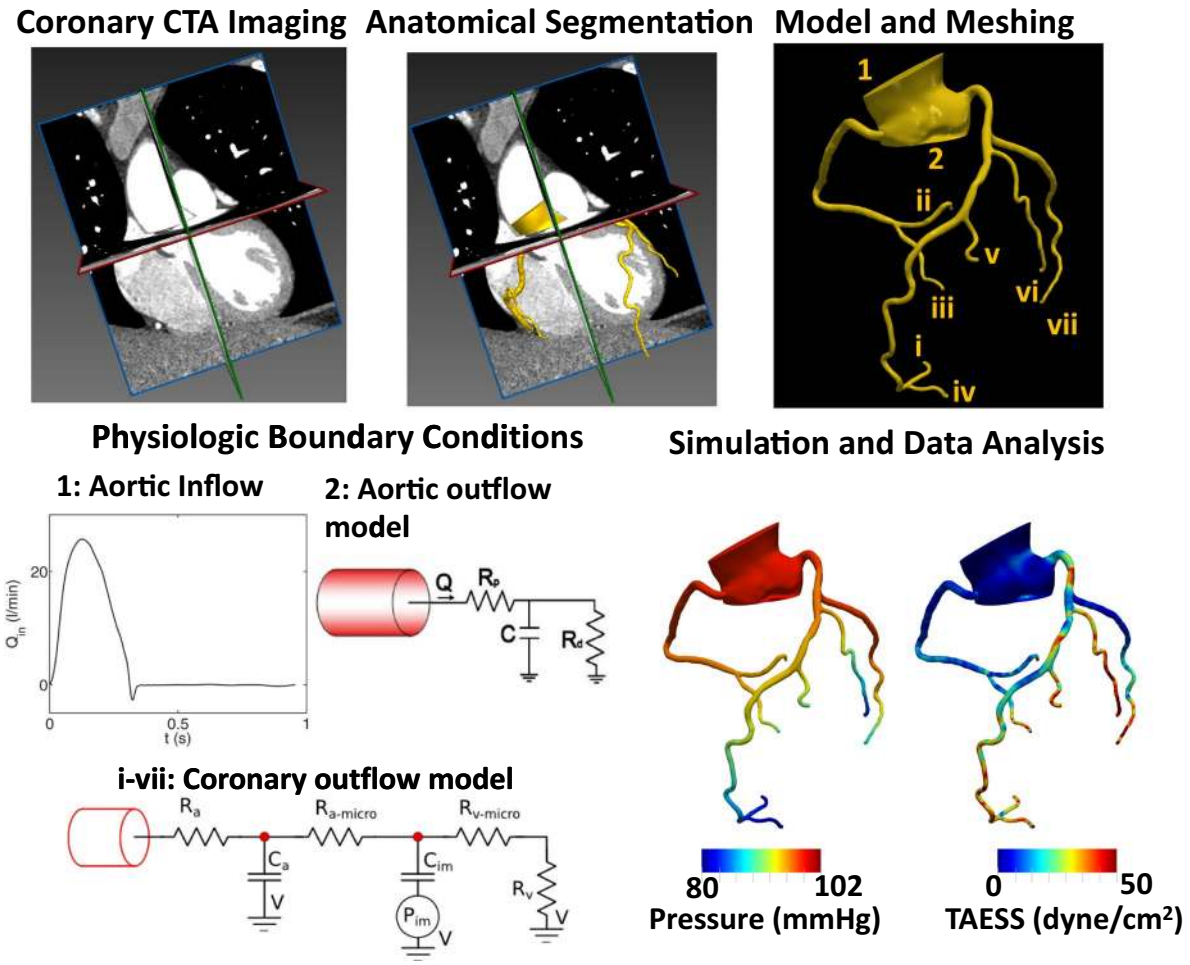

Fig. 2 Elements of patient-specific computational fluid dynamics (CFD) modeling: Coronary CTA imaging acquisition, anatomical segmentation of the coronary tree, 3D model reconstruction and meshing, physiologic boundary condition assignment and simulation and data analysis. In this figure, time-averaged pressure drop in the coronary artery tree and time averaged endothelial shear stress (TAESS) is shown as the results extracted from the CFD calculations

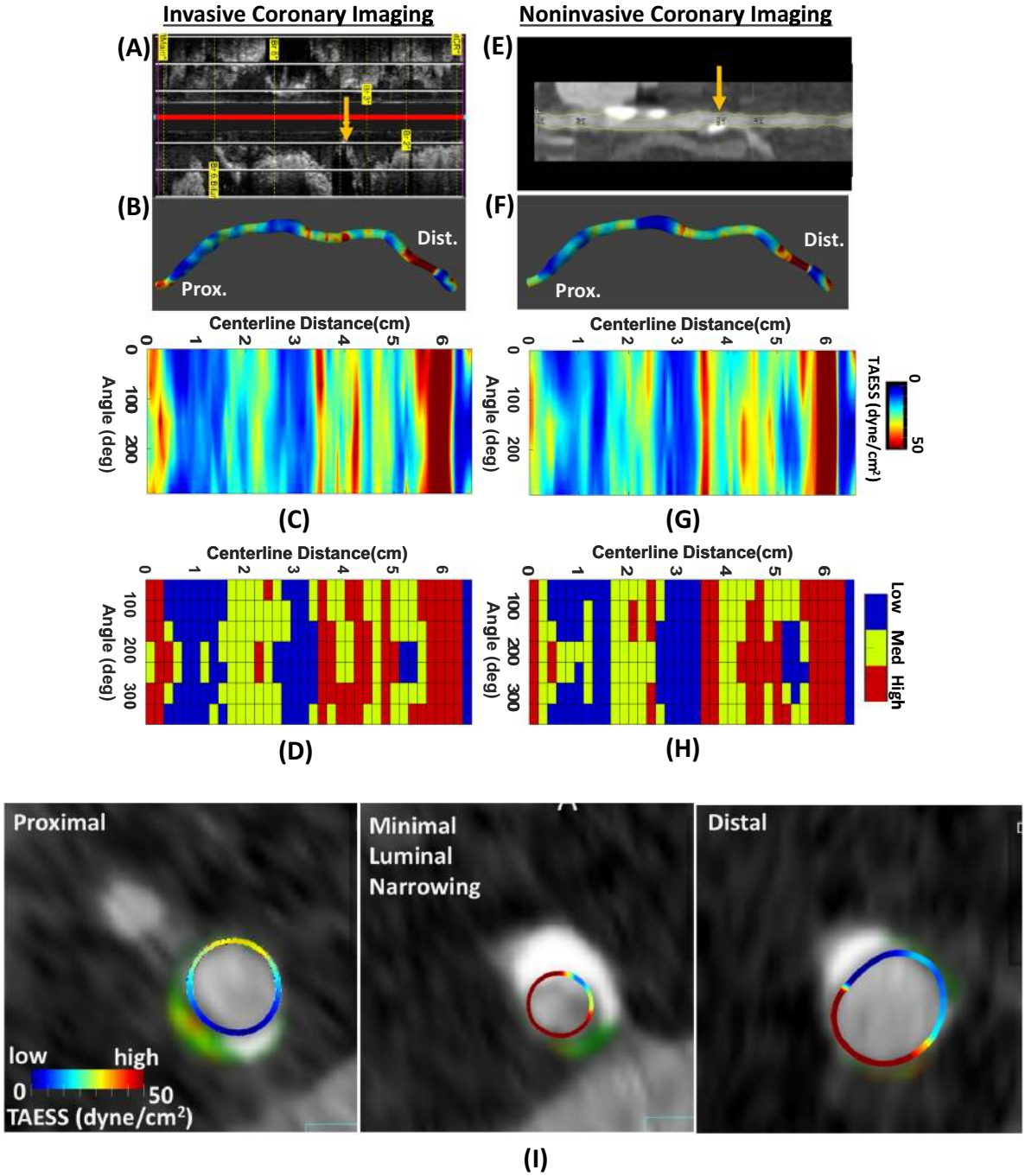

Fig. 3 A representative comparison of TAESS calculating based on invasive IVUS and coronary CTA imaging. Long-axis view of left anterior descending (LAD) based on IVUS and CTA with location of plaque marked with yellow arrows (**a**, **e**). 3D anatomy reconstruction with TAESS mapped on the LAD (**b**, **f**). The "unrolled" 360° values of continuous TAESS (**c**, **g**) and categorical low, medium and high TAESS (**d**, **h**). Short-axis view of a lesion in LAD on CTA with shear stress and plaque morphology mapped at the proximal, minimal luminal narrowing and distal to the narrowing along the lesion. Colors in the plaque morphology represent dense calcium (white), necrotic core (red), fibrous fatty (light green) and fibrous (dark green)

caused by progression and/or disruption of non-calcified plaques and locations with previously no significant obstructive CAD [56]. Since coronary CTA is now widely endorsed as the primary diagnostic imaging modality for patients with stable chest pain, a comprehensive investigation on association of ESS based on serial coronary CTA and natural history of CAD and identification of future culprit lesions would be of a very high value. These studies open an avenue

to apply CTA as an alternative non-invasive imaging modality to study ESS in a larger population where CAD management could be reexamined—being medical therapy, revascularization or both. For example, interaction of medical therapy such as statins and hemodynamic milieu (e.g. ESS) will inform us in which patients would medical therapy be effective by reducing blood cholesterol, preventing atherogenesis, improvement of endothelial cell function and hence physiologic ESS (Fig. 4). In fact, in limited number of few patients, previous studies have shown the potential of CTA as an imaging modality coupled with CFD to model LDL accumulation in a left coronary artery [57] as well as 3D models of plaque formation and progression [58].

Axial stress-CT

In a cylindrical shaped object such as coronary arteries, an axial stress is referred to the longitudinal direction of the vessel exposed to cylindrical blood flow pressure and cardiac motion. Axial stress is the least studied biomechanical force. However, when coronary arteries develop a plaque, due to the obstruction, the flow generates a pressure gradient across the lesion resulting in increased axial stress (referred to as axial plaque stress or APS) and overall plaque strain that may contribute to rupture [59, 60]. APS occurs at magnitudes 10^3 to 10^4 times higher than ESS for different degrees of stenosis and thus may be the biomechanical factor contributing to plaque rupture. APS is difficult to measure in-vivo and has not been well studied compared to ESS and circumferential stress. In a recent study, patients with stable angina and suspected CAD, APS calculated based on CTA has been shown to be significantly higher in the upstream segment of upstream-dominant lesions and in the downstream segment of downstream-dominant lesions implying that APS characterizes the stenotic segment and has a strong relationship with lesion geometry [22].

Along with this concept plaque structural stress (PSS) is a biomechanical stress located inside the body of an atherosclerotic plaque or the arterial wall when vessels expand and stretch due to higher arterial pressure. Since PSS involves tissue and solid biomechanics, it is also determined partly by plaque composition, morphology and material properties. Therefore, it demands FEA computational modeling to calculate the structural stress in the plaque. Localized high PSS levels have shown to result in thrombosis and sudden ischemic clinical events [21]. PSS studies have only been done based on invasive coronary angiograms cross-sections and IVUS where detailed plaque morphology as well as coronary wall can be assessed [21, 61]. Future advances with more accurate assessment of coronary wall and plaque morphology based on coronary CTA may enable PSS calculations.

Elements of computational fluid dynamics modeling and advances

As mentioned briefly above, Navier–Stokes equations, are a set of nonlinear equations that describe the blood flow in 3D. However, these governing equations can only be solved analytically under special circumstances such as steady or pulsatile flow in an idealized circular cylindrical geometries. For a realistic patient-specific model of the human coronary arteries however, a robust numerical method (or CFD) must be used instead to approximate the governing

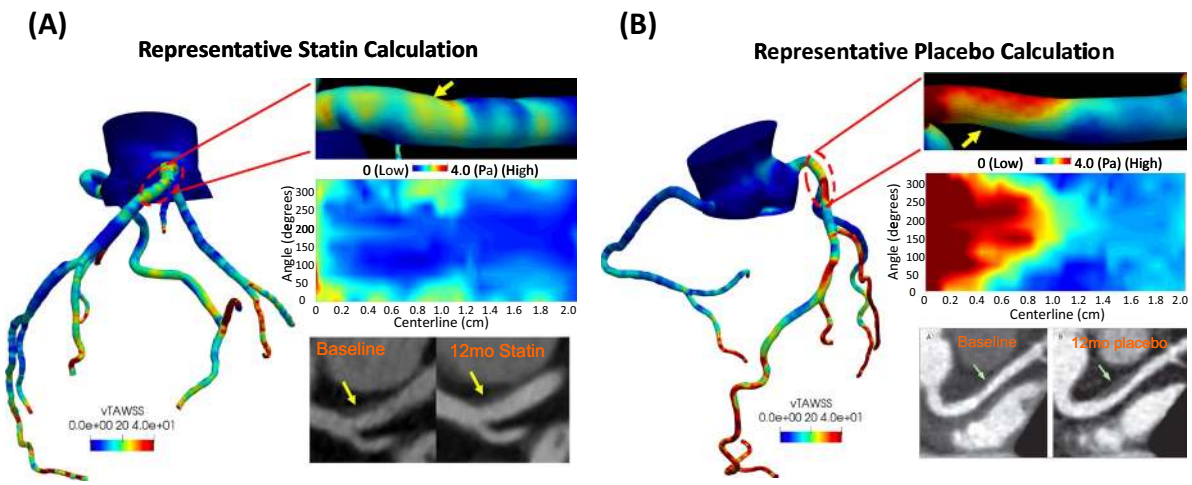

Fig. 4 Calculation of shear stress and studying the effect of statin therapy on distribution of TAESS. A representative calculation of TAESS mapped on the coronary tree based on baseline CT imaging showing low ESS has resulted in progression of CAD in patient randomized to placebo therapy (A) whereas despite the presence of low ESS in the baseline models, the patient's plaque on statin (B) therapy did not progress

equations providing solutions to velocity and pressure at a finite number of points. This requires solving millions of nonlinear partial differential equations simultaneously and iteratively for thousands of small time steps in a cardiac cycle. These equations are not sufficient to solve for blood flow and there are multiple elements that are required in this process [62]: (i) image-based anatomy geometrical construction (ii) proper mesh generation (iii) realistic boundary conditions and (iv) blood properties and rheology (Table 1).

Image-based anatomy geometrical construction

The characteristics of blood flow in the coronary arteries are strongly dependent on the 3D curvature, the presence of branches and bifurcations, and lumen shape including plaque geometry as well as flow pulsatility. These parameters introduce complex hemodynamic features and flow structures such as secondary flow, and flow separations—playing a critical role in assessment of local hemodynamics such as ESS and APS. Therefore, the more complete anatomical information that can be extracted from coronary images, the more realistic models can mimic the physiology in the arteries. Hence, coronary CTA is an ideal candidate to capture the 3D anatomy of the coronary tree. Coronary anatomy geometries of the lumen can be reconstructed by segmentation of each major coronary artery with visible branches limited by the CTA resolution where left and right sides are connected by the ascending aorta to connect the full coronary tree (Fig. 2). This segmentation involves extracting the topology of the coronary artery tree, identifying and segmenting plaque lesions and borders in each vessel and extracting the luminal boundary. These segmentation tools including commercial software packages such as QAngioCT [63] (Leiden, Netherlands) and Syngo.via (Siemens Medical Solutions, USA) have been shown to have a high accuracy and validated to be used clinically.

Mesh generation procedure

For CFD to solve the blood flow, the geometry needs to be divided into many smaller connected meshing elements representing the volume of the blood within the region of interest. In this meshing process, the individual grid spacing, or mesh size, is determined by the complexity of the arteries of interest as well as the balance of spatial and time resolution for a stable convergent simulation. For example, a finer grid spacing should be assigned for regions where larger gradients in the velocity profile are expected. These regions include, higher curvature, branching points and stenosis. The optimal mesh size needs to be also determined by a mesh convergence analysis to demonstrate that further mesh refinement will not result in significant changes to the estimation of target hemodynamic factor such as ESS.

Boundary conditions

Imposing realistic patient-specific boundary conditions is another essential element in CFD simulations of blood flow. Incorrect inlet and outlet boundary conditions will result in unrealistic and wrong representation of coronary artery physiology. For example, in simulations with steady flow, time variation of pulsatile flow is neglected. In invasive imaging based CFD modeling, the time averaged inlet blood flow information can be obtained by using thrombolysis in myocardial infarction (TIMI) frame count [64]. Although less widely available, the inlet flow information can be obtained by intra coronary Doppler ultrasound blood flow velocity measurements providing the entire waveform information [65]. However, in CTA when invasive measurements are not available, cardiac output may be calculated using dynamic coronary CTA in multiple phases based on imaging [66] to prescribe the inflow boundary condition at the aortic level. In the absence of dynamic (or phasic) CTA and availability of a proximate time ejection fraction measured by echocardiogram, the cardiac output can be calculated by the left ventricle volume (extracted from CTA) and ejection fraction. Once, the cardiac output is measured and prescribed at the inlet (the aortic root), the model can be solved using optimized flow solvers for cardiovascular systems to calculate the flow distribution in the coronary tree [67]. However, ideally, patient-specific data should be used to determine the flow re-distribution obtained during computed tomography perfusion [68], transluminal flow encoding equations [69] or myocardial volume [70]. Another widely used methodology is the application of scaling laws. Various scaling laws are available that relate the local diameter of the artery to the average velocity and flowrates [71–74].

The outlet boundary condition is generally set as constant pressure to regular the flow distribution. However, to model the downstream flow of ascending aorta and circulatory system, a lump parameter network (LPN) model can be used to match the patient's measured mean brachial pressure at the time of scan. In addition, assignment of coronary outlet boundary conditions can be done such that unique resistance values for each outlet, based on morphometry laws relating form and function optimized previously [67, 75]. The results shown in this review were obtained by implementing the described LPN boundary conditions (Fig. 2).

Coronary arteries' pulsatile circulation is unique in the body as it is out of phase from the rest of the circulatory system. In the recent years, increasing effort in recreating the correct waveform and capturing the phase have been studied to analyze the temporal variation of hemodynamic factors including the shear stress [76, 77]. Suitable modifications to

Table 1 CFD modeling challenges and potential techniques to address them

CFD modeling		Current challenges and limitations	Opportunities to address
CTA Image acquisition		Lower spatial resolution for coronary CTA is ~ 0.3 mm limiting their use to coronary arteries of 1.5 mm or greater in diameter [101] Sever motion artifacts, stair-step artifacts, image noise, calcium blooming or beam-hardening effect in stented regions may lead to non-diagnostic CTA images [94] Imaged coronary anatomy may not be reflective of the true phasic changes of vessel diameter	Implementation of automatic algorithms and iterative reconstructions to correct for motion artifacts [102], calcium blooming and stents [103, 104], image noises etc. ECG-gated dynamic CTA imaging will capture phasic anatomic changes of the coronaries, however this will introduce more radiation [105] Elastic wall modeling may be implemented using FSI simulations to capture the wall movement [66]
Segmentation and 3D model reconstruction		Imaging artifacts make it difficult to segment the images and detect the true lumen borders Segmentation of the coronary artery lumen, plaque and wall is a tedious and time-consuming process	Implementation of clinically used semi-automatic algorithms have improved quantitative luminal assessment [63, 106] Implementation of fully automized segmentation tools utilizing deep learning algorithm may increase the accuracy and decease labor intensive segmentation process [95]
Fluid dynamic simulation	Mesh generation	Quality control of the generated mesh is challenging [107] and a crucial step to ensure that the mesh reflects the domain and geometry that bounds the blood flow	Mesh generation algorithm developers continuously update for better quality adaptive mesh generation [108, 109] for unconventional geometries such as the coronaries, carotids [110] and the heart
	Boundary conditions	Realistic patient-specific boundary conditions at the time of scan is an essential step in CFD modeling. However, access to such data is limited to imaging protocol as well as the invasive nature of the procedure	Invasive and in-vivo measurement of pressure during the FFR procedure provides a patient-specific pressure measurement in the coronary arteries. Volumetric flowrate can also be measured using ultrasound and doppler imaging [111, 112] Non-invasive image-based alternatives may be the use of contrast information from CTA based on transluminal attenuation gradient [24, 69] Inlet conditions can be prescribed from CTA-based calculated cardiac output as a total flowrate prescribed at the inlet of the aortic root [66] Lumped parameter (0 or 1-order) models can be used as boundary conditions. The lumped parameters (e.g., resistance, compliance, etc.) may be tuned via numerical optimization and sensitivity analysis [79, 113]
	Blood rheology	Blood by nature is a non-Newtonian fluid where its viscosity depends on shear rate. Non-Newtonian blood simulations require longer computational time to stabilize and require finer boundary layers to resolve the flow	Blood flow in large vessels such as coronary arteries generally behave as a Newtonian fluid, therefore most of CFD studies assume a Newtonian fluid in the coronaries Robust fluid solvers have implemented various constitutive non-Newtonian models such as Carreau–Yasuda [91], Quemada [92] and Herschel-Bukley [93]

Table 1 (continued)

CFD modeling	Current challenges and limitations	Opportunities to address
FSI coupling	FSI techniques although capture the compliant wall of the coronaries, they require expensive computational simulations. Traditional ALE [82] methods require tracking of the fluid and structural remeshing costing expensive computations	Alternative FSI techniques include CMM [80] where not large deformation is assumed. IBM [83, 84] techniques is another alternative method which treats the fluid points as stationary with moving boundaries

the boundary conditions such as including a pressure source in the LPN model can be implemented to impose an out of phase with the systemic circulation. Including an intramyocardial pressure source to impede flow during systole and relax during diastole adjusts the coronary circulation phase [78]. In addition, appropriate time dependent LPN at the outlets of coronary arteries can also capture the difference between phasic coronary flow in the left and right coronaries [79].

Lastly, in coronary models with rigid geometry assumptions, a no slip boundary conditions at the wall is prescribed to ensure zero velocity of fluid flow at the wall. Although coronary artery walls are elastic by nature, the majority of the studies have been implemented using rigid wall assumptions. Simulations with elastic models are computationally expensive calculations. Recent FSI investigations using coupled momentum method (CMM) [80]—treating the fixed fluid meshes with a solid boundary as a linear membrane—have shown that although phasic ESS has different patterns in the rigid and elastic wall models of the coronary arteries, time-averaged ESS in each cardiac cycle showed a negligible difference [66, 81]. Therefore, rigid models with no FSI modeling are justified to be used to solve the flow in the coronaries. Other FSI techniques include Arbitrary Lagrangian–Eulerian (ALE) [82] method which tracks boundaries and interfaces of both fluid and structural computational domains during each iteration, requires both the lumen and wall mesh domains and, are computationally more expensive simulations. Another alternative FSI technique includes immersed boundary method (IBM) [83, 84] using Cartesian grids where the fluid meshes are fixed with boundaries defined by a set of moving Lagrangian points. The IBM technique however is not efficient for coronary simulations where there are unused grids that still have to be computational solved but are not I the fluid domain. Prescribed heart motion has been used previously for simulating the blood flow in left [85] and right coronary arteries [86, 87], however, to capture heart motion and large deformations during a cardiac cycle, more efficient and robust FSI techniques are necessary. While rigid model assumptions are justified for calculation of ESS, FSI modeling is the only means of coupling ESS and PSS requiring inclusion of both lumen and coronary wall geometires [21, 88].

Blood properties and rheology

Generally, CFD models of blood flow in coronary arteries assume that blood is a Newtonian fluid with constant viscosity. However, blood comprises a mixture of red blood cells, white blood cells, platelet, and plasma consisting of both solid and liquid phases. Therefore, blood exhibits non-Newtonian properties such as shear-thinning where its apparent viscosity lowers at higher shear rates. While

Newtonian assumptions are generally acceptable in larger arteries such as the aorta and coronaries, it may not be as accurate in the setting of complex flow patterns, particularly at the sight of severe stenosis or stented regions in the coronary arteries [89, 90]. There are multiple constitutive models of shear-thinning non-Newtonian fluids such as the Carreau–Yasuda [91], Quemada [92] and Herschel-Bukley [93] models that should be studied and used according to the shear rate imposed on the blood cells.

Future directions and limitations of CTA-based computational modeling

Imaging artifacts and lower resolution of CTA may affect CTA interpretability, including calcification, motion and misregistration and beam hardening effect caused by the potential stents in the arteries [94]. Since CFD modeling heavily relies on accurate anatomical reconstruction of the coronary tree, these artifacts may limit the accuracy of the models. One way to lower errors and segmentation time is to develop optimized, automated segmentation algorithms. With the availability of large dataset, recent deep learning convolutional neural network development have shown promising techniques to automatically identify coronary plaques and stenosis level based on coronary CTA [95, 96]. This is a great step towards segmentation of the lumen in the entire coronary tree [97]. Appropriate physiologic boundary conditions is another essential component to model patient-specific models. The more generic assumptions the model includes, the more deviation the model may have from the individual patient's physiologic conditions.

Clinical implementation of computational modeling is another limitation of image-based physiologic modeling. At the current stage, computational modeling is not a trivial bed-side application that can provide real-time information to the physicians. Accurate modeling requires the expertise of trained engineers to reconstruct models from medical imaging, run theoretical validated simulations and extract the relevant data. Although image-based computational modeling has advanced immensely in the recent years (e.g. FFR_{CT}), it is still limited by the computational time, segmentation, reconstruction and post-processing which requires 3–8 h for each patient-specific coronary tree. Therefore, optimized flow solvers for cardiovascular problems are required to efficiently solve the flow with high accuracy [98]. Nevertheless, this appears to be changing rapidly with continuous increase in computational power and availability. Simplification of CFD assumptions including steady flow versus pulsatile flow would allow for faster implementation of the arteries, yet, there is always an optimization battle between accurate modeling, local flow details captured by the models and computational time. Furthermore, other technical advances such as deep-learning estimation of CFD-based parameters is a novel way of decreasing computational time. For instance, as a growing body of evidence has validated the diagnostic accuracy of FFR_{CT} techniques compared with invasive FFR, the data acquired can be utilized to train deep-learning networks to estimate the FFR based on CT images (FFR_{ML}; ML: machine learning) [99, 100].

Conclusion

In this review we examined the state-of-the-art evidence of utilization of coronary CTA and assessing physiologic conditions relative to the natural history of coronary plaque. We showed that coronary CTA has been successfully used as a standard noninvasive imaging modality to provide FFR_{CT}—less affected on local geometry— as a physiological parameter to identify flow limiting lesions. However, since ESS, APS and PSS are all biomechanical factors that are very sensitive to the local geometry, more accurate CFD modeling elements need to be implemented to calculate and report these physiologic parameters. Improved non-invasive plaque imaging and computational characterization will be necessary for an accurate assessment and primary prevention of clinically significant vulnerable plaque. Thus, although CTA-based assessment of these parameters may have high impact for a larger group of patients, validation with invasive imaging provides the necessary insight in improvement of technical and clinical approaches.

Compliance with ethical standards

Conflict of interest All authors declare that they have no conflict of interest.

References

1. Maurovich-Horvat P, Ferencik M, Voros S, Merkely B, Hoffmann U (2014) Comprehensive plaque assessment by coronary CT angiography. Nat Rev Cardiol 11:390–402
2. WHO (2019) Cardiovascular diseases (CVDs). WHO, Geneva
3. Khavjou O, Phelps D, Leib A (2016) Projections of cardiovascular disease prevalence and costs: 2015–2035. RTI Int. 38:1–54
4. Hadamitzky M et al (2013) Optimized prognostic score for coronary computed tomographic angiography: results from the CONFIRM registry (COronary CT angiography evaluation for clinical outcomes: An international multicenter registry). J Am Coll Cardiol 62:468–476
5. Hoffmann U et al (2017) Prognostic value of noninvasive cardiovascular testing in patients with stable chest pain: insights from the PROMISE Trial (Prospective Multicenter Imaging Study for Evaluation of Chest Pain). Circulation 135:2320–2332

6. Ferencik M et al (2018) Use of high-risk coronary atherosclerotic plaque detection for risk stratification of patients with stable chest pain: a secondary analysis of the promise randomized clinical trial. JAMA Cardiol 3:144–152
7. Williams MC et al (2019) Coronary artery plaque characteristics associated with adverse outcomes in the SCOT-HEART study. J Am Coll Cardiol 73:291–301
8. Chang HJ et al (2018) Coronary atherosclerotic precursors of acute coronary syndromes. J Am Coll Cardiol 71:2511–2522
9. Wentzel JJ et al (2012) Endothelial shear stress in the evolution of coronary atherosclerotic plaque and vascular remodelling: current understanding and remaining questions. Cardiovasc Res 96:234–243
10. Thondapu V et al (2017) Basic science for the clinician: biomechanical stress in coronary atherosclerosis: Emerging insights from computational modelling. Eur Heart J 38:81–92
11. Ford TJ et al (2017) Physiological predictors of acute coronary syndromes: emerging insights from the plaque to the vulnerable patient. JACC Cardiovasc Interv 10:2539–2547
12. Loewe C, Stadler A (2014) Computed tomography assessment of hemodynamic significance of coronary artery disease: CT perfusion, contrast gradients by coronary CTA, and fractional flow reserve review. J Thorac Imaging 29:163–172
13. Pijls NHJ et al (1996) Measurement of fractional flow reserve to assess the functional severity of coronary-artery stenoses. N Engl J Med 334:1703–1708
14. Tonino PA et al (2009) Fractional flow reserve versus angiography for guiding percutaneous coronary intervention. N Engl J Med 360:333–340
15. Melikian N et al (2010) Fractional flow reserve and myocardial perfusion imaging in patients with angiographic multivessel coronary artery disease. JACC Cardiovasc Interv 3:307–314
16. Johnson NP, Kirkeeide RL, Gould KL (2013) Coronary anatomy to predict physiology fundamental limits. Circ Cardiovasc Imaging 6:817–832
17. Hoogendoorn A et al (2019) Multidirectional wall shear stress promotes advanced coronary plaque development: comparing five shear stress metrics. Cardiovasc Res 116:1136–1146. https://doi.org/10.1093/cvr/cvz212
18. Stone PH et al (2012) Prediction of progression of coronary artery disease and clinical outcomes using vascular profiling of endothelial shear stress and arterial plaque characteristics: the PREDICTION study. Circulation 126:172–181
19. Stone PH et al (2018) Role of low endothelial shear stress and plaque characteristics in the prediction of nonculprit major adverse cardiac events: the PROSPECT study. JACC Cardiovasc Imaging 11:462–471
20. Samady H et al (2011) Coronary artery wall shear stress is associated with progression and transformation of atherosclerotic plaque and arterial remodeling in patients with coronary artery disease. Circulation 124:779–788
21. Costopoulos C et al (2019) Impact of combined plaque structural stress and wall shear stress on coronary plaque progression, regression, and changes in composition. Eur Heart J 40:1411–1422. https://doi.org/10.1093/eurheartj/ehz132
22. Choi G et al (2015) Coronary artery axial plaque stress and its relationship with lesion geometry application of computational fluid dynamics to coronary CT angiography. JACC Cardiovasc Imaging 8:1156–1166
23. Wong DTL et al (2013) Transluminal attenuation gradient in coronary computed tomography angiography is a novel noninvasive approach to the identification of functionally significant coronary artery stenosis: a comparison with fractional flow reserve. J Am Coll Cardiol 61:1271–1279
24. Lardo AC et al (2015) Estimating coronary blood flow using CT transluminal attenuation flow encoding: formulation, preclinical validation, and clinical feasibility. J Cardiovasc Comput Tomogr 9:559–566
25. Lu MT et al (2016) Noninvasive FFR derived from coronary CT angiography. Management and outcomes in the PROMISE trial. JACC Cardiovasc. Imaging. https://doi.org/10.1016/j.jcmg.2016.11.024
26. Park JB et al (2016) Computational fluid dynamic measures of wall shear stress are related to coronary lesion characteristics. Heart 102:1655–1661
27. Nørgaard BL et al (2014) Diagnostic performance of noninvasive fractional flow reserve derived from coronary computed tomography angiography in suspected coronary artery disease: The NXT trial (Analysis of Coronary Blood Flow Using CT Angiography: Next Steps). J Am Coll Cardiol 63:1145–1155
28. Pijls NHJ et al (2007) Percutaneous coronary intervention of functionally nonsignificant stenosis. 5-Year follow-up of the DEFER study. J Am Coll Cardiol 49:2105–2111
29. Gould KL (1978) Pressure-flow characteristics of coronary stenoses in unsedated dogs at rest and during coronary vasodilation. Circ Res 43:242–253
30. Xing Z, Pei J, Huang J, Hu X, Gao S (2019) Diagnostic performance of QFR for the evaluation of intermediate coronary artery stenosis confirmed by fractional flow reserve. Braz J Cardiovasc Surg 34:165–172
31. Westra J et al (2018) Evaluation of coronary artery stenosis by quantitative flow ratio during invasive coronary angiography: the WIFI II study (Wire-Free Functional Imaging II). Circ Cardiovasc Imaging 11:1–8
32. Baumann S et al (2018) Instantaneous wave-free ratio (iFR®) to determine hemodynamically significant coronary stenosis: a comprehensive review. World J Cardiol 10:267–277
33. Götberg M et al (2017) Instantaneous wave-free ratio versus fractional flow reserve to guide PCI. N Engl J Med 376:1813–1823
34. Davies JE et al (2017) Use of the instantaneous wave-free ratio or fractional flow reserve in PCI. N Engl J Med 376:1824–1834
35. Johnson NP et al (2013) Does the instantaneous wave-free ratio approximate the fractional flow reserve? J Am Coll Cardiol 61:1428–1435
36. Lee JM et al (2018) Prognostic implication of thermodilution coronary flow reserve in patients undergoing fractional flow reserve measurement. JACC Cardiovasc Interv 11:1423–1433
37. Gaur S et al (2014) Fractional flow reserve derived from coronary CT angiography: variation of repeated analyses. J Cardiovasc Comput Tomogr 8:307–314
38. National Institute for Health and Care Excellence (NICE) (2017) HeartFlow FFRCT for estimating fractional flow reserve from coronary CT angiography. Medical technologies guidance, vol 32. NICE, London
39. National Institute for Health and Care Excellence (NICE) (2016) Chest pain of recent onset: assessment and diagnosis. NICE, London
40. Eshtehardi P et al (2012) Association of coronary wall shear stress with atherosclerotic plaque burden, composition, and distribution in patients with coronary artery disease. J Am Heart Assoc 1:e002543–e002543
41. Chatzizisis YS et al (2009) Attenuation of inflammation and expansive remodeling by Valsartan alone or in combination with Simvastatin in high-risk coronary atherosclerotic plaques. Atherosclerosis 203:387–394
42. Fry DL (1968) Acute vascular endothelial changes associated with increased blood velocity gradients. Circ Res 22:165–197
43. Caro CG, Fitz-Gerald JM, Schroter RC (1971) Atheroma and arterial wall shear. Observation, correlation and proposal of a shear dependent mass transfer mechanism for atherogenesis. Proc R Soc Lond B 177:109–159

44. Ha CH et al (2013) Inhibitory effect of soluble RAGE in disturbed flow-induced atherogenesis. Int J Mol Med 32:373–380
45. Gimbrone MA (1999) Endothelial dysfunction, hemodynamic forces, and atherosclerosis. Thromb Haemost 82:722–726
46. Gimbrone MAG, García-Cardeña G (2015) Vascular endothelium, hemodynamics, and the pathobiology of atherosclerosis. Cardiovasc Pathol 22:9–15
47. Gijsen FJH et al (2008) Strain distribution over plaques in human coronary arteries relates to shear stress. Am J Physiol Hear Circ Physiol 295:1608–1614
48. Chatzizisis YS et al (2011) Augmented expression and activity of extracellular matrix-degrading enzymes in regions of low endothelial shear stress colocalize with coronary atheromata with thin fibrous caps in pigs. Circulation 123:621–630
49. Chatzizisis YS et al (2007) Role of endothelial shear stress in the natural history of coronary atherosclerosis and vascular remodeling. Molecular, cellular, and vascular behavior. J Am Coll Cardiol 49:2379–2393
50. Stone PH et al (2003) Effect of endothelial shear stress on the progression of coronary artery disease, vascular remodeling, and in-stent restenosis in humans: in vivo 6-month follow-up study. Circulation 108:438–444
51. Stone PH et al (2007) Regions of low endothelial shear stress are the sites where coronary plaque progresses and vascular remodelling occurs in humans: an in vivo serial study. Eur Heart J 28:705–710
52. Kumar A et al (2018) High coronary shear stress in patients with coronary artery disease predicts myocardial infarction. J Am Coll Cardiol 72:1926–1935
53. Lee JM et al (2019) Identification of high-risk plaques destined to cause acute coronary syndrome using coronary computed tomographic angiography and computational fluid dynamics. JACC Cardiovasc Imaging 12:1032–1043
54. Han D et al (2016) Relationship between endothelial wall shear stress and high-risk atherosclerotic plaque characteristics for identification of coronary lesions that cause ischemia: a direct comparison with fractional flow reserve. J Am Heart Assoc 5:1–9
55. Bech GJW et al (2001) Fractional flow reserve to determine the appropriateness of angioplasty in moderate coronary stenosis: a randomized trial. Circulation 103:2928–2934
56. Parikh NI et al (2010) Long-term trends in myocardial infarction incidence and case-fatality in the national heart. Lung Blood Inst Framingham Heart Study 119:1203–1210
57. Olgac U, Poulikakos D, Saur SC, Alkadhi H, Kurtcuoglu V (2009) Patient-specific three-dimensional simulation of LDL accumulation in a human left coronary artery in its healthy and atherosclerotic states. Am. J. Physiol. Hear. Circ. Physiol. 296:H1969–H1982
58. Parodi O et al (2012) Patient-specific prediction of coronary plaque growth from CTA angiography: a multiscale model for plaque formation and progression. IEEE Trans Inf Technol Biomed 16:952–965
59. Li ZY et al (2009) The mechanical triggers of plaque rupture: shear stress vs pressure gradient. Br J Radiol 82:S39–S45
60. Slagger CJ et al (2005) The role of shear stress in the destabilization of vulnerable plaques and related therapeutic implications. Nat Clin Pract Cardiovasc Med 2:456–464
61. Brown AJ et al (2016) Role of biomechanical forces in the natural history of coronary atherosclerosis. Nat Rev Cardiol 13:210–220
62. Gijsen F et al (2019) Expert recommendations on the assessment of wall shear stress in human coronary arteries: existing methodologies, technical considerations, and clinical applications. Eur Heart J 40:3421–3433
63. Boogers MJ et al (2010) Automated quantification of stenosis severity on 64-slice CT: a comparison with quantitative coronary angiography. JACC Cardiovasc Imaging 3:699–709
64. Dodge JT et al (1998) Impact of injection rate on the thrombolysis in myocardial infarction (TIMI) trial frame count. Am J Cardiol 81:1268–1270
65. Tanedo JS et al (2001) Assessing coronary blood flow dynamics with the TIMI frame count method: comparison with simultaneous intracoronary Doppler and ultrasound. Catheter Cardiovasc Interv 53:459–463
66. Eslami P et al (2019) Effect of wall elasticity on hemodynamics and wall shear stress in patient-specific simulations in the coronary arteries. J. Biomech. Eng. 142(2):0245031–02450310
67. Updegrove A et al (2017) SimVascular: an open source pipeline for cardiovascular simulation. Ann Biomed Eng 45:525–541
68. Rossi A et al (2014) Stress myocardial perfusion imaging with multidetector CT. Radiology 270:25–46
69. Eslami P et al (2015) Computational study of computed tomography contrast gradients in models of stenosed coronary arteries. J Biomech Eng 137:091002
70. Kurata A et al (2015) Quantification of the myocardial area at risk using coronary CT angiography and Voronoi algorithm-based myocardial segmentation. Eur Radiol 25:49–57
71. Murray CD (1926) The physiological principle of minimum work. The vascular systems and the cost of blood volume. J Gen Physiol 12:445
72. Zhou Y, Kassab GS, Molloi S (2002) In vivo validation of the design rules of the coronary arteries and their application in the assessment of diffuse disease. Phys Med Biol 47:977–993
73. Kassab GS (2006) Scaling laws of vascular trees: of form and function. Am J Physiol Heart Circ Physiol 290:894–903
74. van der Giessen AG et al (2011) The influence of boundary conditions on wall shear stress distribution in patients specific coronary trees. J Biomech 44:1089–1095
75. Tran JS, Schiavazzi DE, Ramachandra AB, Kahn AM, Marsden AL (2016) Automated tuning for parameter identification and uncertainty quantification in multi-scale coronary simulations. Comput Fluids 142:128–138
76. Barlis P et al (2015) Reversal of flow between serial bifurcation lesions: insights from computational fluid dynamic analysis in a population-based phantom model. EuroIntervention 11:e1–e3
77. Davies PF (2009) Hemodynamic shear stress and the endothelium in cardiovascular pathophysiology. Nat Clin Pract Cardiovasc Med 6:16–26
78. Kim HJ et al (2010) Patient-specific modeling of blood flow and pressure in human coronary arteries. Ann Biomed Eng 38:3195–3209
79. Sankaran S et al (2012) Patient-specific multiscale modeling of blood flow for coronary artery bypass graft surgery. Ann Biomed Eng 40:2228–2242
80. Figueroa CA, Vignon-Clementel IE, Jansen KE, Hughes TJR, Taylor CA (2006) A coupled momentum method for modeling blood flow in three-dimensional deformable arteries. Comput Methods Appl Mech Eng 195:5685–5706
81. Torii R, Oshima M, Kobayashi T, Takagi K, Tezduyar TE (2008) Fluid-structure interaction modeling of a patient-specific cerebral aneurysm: influence of structural modeling. Comput Mech 43:151–159
82. Hecht F, Pironneau O (2017) An energy stable monolithic Eulerian fluid-structure finite element method. Int J Numer Methods Fluids 85:430–446
83. Peskin CS, Peskin CS (2002) Numerica : The immersed boundary method. The immersed boundary method. Acta Numer 11:479–517

84. Seo JH, Mittal R (2011) A sharp-interface immersed boundary method with improved mass conservation and reduced spurious pressure oscillations. J Comput Phys 230:7347–7363
85. Prosi M, Perktold K, Ding Z, Friedman MH (2004) Influence of curvature dynamics on pulsatile coronary artery flow in a realistic bifurcation model. J Biomech 37:1767–1775
86. Torii R et al (1965) Fluid–structure interaction analysis of a patient-specific right coronary artery with physiological velocity and pressure waveforms. Commun Numer Methods Eng 90:443–445
87. Torii R et al (2009) The effect of dynamic vessel motion on haemodynamic parameters in the right coronary artery: a combined MR and CFD study. Br. J. Radiol. 82:S24–S32
88. Mundi S et al (2018) Endothelial permeability, LDL deposition, and cardiovascular risk factors-A review. Cardiovasc Res 114:35–52
89. Anssari-Benam A, Bader DL, Screen HRC (2011) A combined experimental and modelling approach to aortic valve viscoelasticity in tensile deformation. J Mater Sci Mater Med 22:253–262
90. Thondapu V et al (2018) Endothelial shear stress 5 years after implantation of a coronary bioresorbable scaffold. Eur Heart J 39:1602–1609
91. Boyd J, Buick JM, Green S (2007) Analysis of the Casson and Carreau-Yasuda non-Newtonian blood models in steady and oscillatory flow using the lattice Botlzmann method. Phys. Fluids 19:93103
92. Quemada D (1978) Rheology of concentrated disperse systems III. General features of the proposed non-Newtonian model. Comparison with experimental data. Rheol Acta 17:643–653
93. Tang HS, Kalyon DM (2004) Estimation of the parameters of Herschel-Bulkley fluid under wall slip using a combination of capillary and squeeze flow viscometers. Rheol Acta 43:80–88
94. Alkadhi H et al (2008) Radiation dose of cardiac dual-source CT: the effect of tailoring the protocol to patient-specific parameters. Eur J Radiol 68:385–391
95. Hong Y et al (2019) Deep learning-based stenosis quantification from coronary CT Angiography. Proc SPIE. https://doi.org/10.1097/CCM.0b013e31823da96d.Hydrogen
96. Zreik M et al (2019) A recurrent CNN for automatic detection and classification of coronary artery plaque and stenosis in coronary CT angiography. IEEE Trans Med Imaging 38:1588–1598
97. Maher G, Wilson N, Marsden A (2019) Accelerating cardiovascular model building with convolutional neural networks. Med Biol Eng Comput 57:2319–2335
98. Zhong L et al (2018) Application of patient-specific computational fluid dynamics in coronary and intra-cardiac flow simulations: challenges and opportunities. Front Physiol 9:742
99. Tesche C et al (2016) Coronary CT angiography-derived fractional flow reserve. Radiology 285:17–33
100. Coenen A et al (2018) Diagnostic accuracy of a machine-learning approach to coronary computed tomographic angiography-based fractional flow reserve result from the MACHINE Consortium. Circ Cardiovasc Imaging 11:1–11
101. Kantor B, Kuzo RS, Gerber TC (2007) Coronary computed tomographic angiography: current and future uses. Hear Metab 34:5–9
102. Ma H et al (2018) Automated quantification and evaluation of motion artifact on coronary CT angiography images. Med Phys 45:5494–5508
103. Li P et al (2018) Blooming artifact reduction in coronary artery calcification by a new de-blooming algorithm: initial study. Sci Rep 8:1–8
104. Halliburton SS, Tanabe Y, Partovi S, Rajiah P (2017) The role of advanced reconstruction algorithms in cardiac CT. Cardiovasc Diagn Ther 7:527–538
105. Nishiyama H et al (2019) Incremental diagnostic value of whole-heart dynamic computed tomography perfusion imaging for detecting obstructive coronary artery disease. J Cardiol 73:425–431
106. Diaz-zamudio M et al (2017) Quantitative plaque features from coronary computed tomography angiography to identify regional ischemia by myocardial perfusion imaging. Eur Heart J 18:499–507
107. Wittek A, Grosland NM, Joldes GR, Magnotta V, Miller K (2016) From finite element meshes to clouds of points: a review of methods for generation of computational biomechanics models for patient-specific applications. Ann Biomed Eng 44:3–15
108. You YH, Kou XY, Tan ST (2015) Adaptive meshing for finite element analysis of heterogeneous materials. Comput Des 62:176–189
109. Si H (2015) TetGen, a quality tetrahedral mesh generator. AMC Trans Math Softw 41:11
110. Seo JH, Eslami P, Caplan J, Tamargo RJ, Mittal R (2018) A highly automated computational method for modeling of intracranial aneurysm hemodynamics. Front Physiol 9:1–12
111. Bishop AH, Samady H (2004) Fractional flow reserve: critical review of an important physiologic adjunct to angiography. Am Heart J 147:792–802
112. Barfett JJ, Fistra J, Mikulis DJ, Krings T (2010) Blood velocity calculated from volumetric dynamic computed scanning of flow phantoms. Invest Radiol 45:10–13
113. Tran JS, Schiavazzi DE, Ramachandra AB, Kahn AM, Marsden AL (2016) Automated tuning for parameter identification and uncertainty quantification in multi-scale coronary simulations. Comput Fluids 27:138–144